PCCP

Accepted Manuscript

ROYAL SOCIETY OF CHEMISTRY

rsc.li/pccp

View Article Online
DOI: 10.1039/C7CP04059H

Analytical solution of the PELDOR inverse problem using the integral Mellin transform

Anna G. Matveeva[1,2]*, Vyacheslav M. Nekrasov[1,2], Alexander G. Maryasov[1]

[1]*Voevodsky Institute of Chemical kinetics and Combustion, 630090 Novosibirsk, Russia*

[2]*Novosibirsk State University, 630090 Novosibirsk, Russia*

Abstract

We describe a new model-free approach to solve the inverse problem in pulsed double electron-electron resonance (PELDOR, also known as DEER) spectroscopy and obtain the distance distribution function between two radicals from time-domain PELDOR data. The approach is based on analytical solutions of the Fredholm integral equations of the first kind using integral Mellin transforms to provide the distance distribution function directly.
The approach appears to confine the noise in the computed distance distribution to short distances and does not introduce systematic distortions. Thus, the proposed analysis method can be a useful supplement to current methods to determine complicated distance distributions.

Introduction

The measured signal in pulsed magnetic resonance is a set of oscillations caused by transitions between different eigenstates, e.g., the free induction decay (FID) or spin-echo signals. Special pulse sequences are used to isolate the frequencies containing useful information. In many cases, it is sufficient to study the spectral composition of the signal by applying the Fourier transform to the time-domain signal. In a pulse electron-electron double resonance method known as PELDOR or DEER, an additional pulse at a second frequency between the main Hahn-echo pulses allows us to see only the dipole-dipole interaction between electron spins [1]. The dipole-dipole interaction of the spins depends on their mutual arrangement and orientation; therefore its study can provide important information on the structural characteristics of molecules. There are several variations of PELDOR using three pulses [1], four pulses [2] and five pulses [3], but their data is processed the same way.

The most important and frequently used application of PELDOR is to determine the distribution of distances between spins. If there is a strictly fixed distance between the spin probes or labels, the ideal signal can be calculated analytically, see below. Its Fourier image is the Pake doublet - a curve with four singularities - two steps and two divergences of the inverse square root type. The presence of a distribution of distances in a radical pair blurs the singularities, which, on the one hand, seriously complicates the direct analysis of the spectra, but, on the other hand, allows us to obtain information not only about the average distance between the labels, but also about the shape of the entire distribution over distances.

In the last 2 decades PELDOR has become very popular [4-10] because of its applications to the study of structures of different biological molecules. Indeed, the PELDOR signal decay contains information about distances between labels over a range of 1.5-8 nm or more.

View Article Online
DOI: 10.1039/C7CP04059H

In the simplest, and most common, case of randomly-oriented pairs of spins without exchange interaction, the normalized intramolecular part of the PELDOR signal decay may be presented as [1]

$$V(T)=\int_0^{\infty}\int_0^{\pi/2} f(r)\cos\left[\frac{\gamma^2\hbar}{r^3}\left(1-3\cos^2\theta\right)T\right]\sin\theta d\theta dr \qquad (1)$$

This is the average of a signal from a pair of weakly-coupled spins with a distance distribution function *f(r)*. The spins have a dipole interaction between them which is described by distance *r* and an angle θ between the inter-spin vector r and the direction of the external magnetic field, γ is the electron gyromagnetic ratio. Thus, the problem of finding the distance distribution function reduces to the solution of Eq.(1) for the unknown *f(r)*. This equation is a particular example of the general Fredholm integral equation of the first kind

$$V(T)=\int_0^{\infty} f(r)K(r,T)dr \text{ with the kernel } K(r,T)=\int_0^{\pi/2}\cos\left[\frac{\gamma^2\hbar}{r^3}\left(1-3\cos^2\theta\right)T\right]\sin\theta d\theta$$

However, it is known that the solution of all Fredholm type I inverse problems is unstable to noise (mathematically ill-posed), so that some regularization algorithm should be used. The first method used to solve the PELDOR inverse problem was to replace the kernel with a step function of (T/r^3) [1]. This method allows reasonable accuracy to determine broad *f(r)*, but it is no longer used. On the basis of this approach, a nonparametric technique to obtain mean distance of wide distance distribution function was suggested in [11].

Today the most popular approach is Tikhonov regularization, which gives a compromise between the smoothness of the desired *f(r)* and the deviation of the calculated *V(T)* from the experimental one [11, 12]. It should be noted that the standard Tikhonov regularization has obvious limitations for recovering distributions with sharp, narrow features when there is a significant noise level [12]. These limitations prompt researchers to look for new approaches to solving the inverse problem.

The modified Tikhonov functional, known as the maximum entropy method [13], is also used to stabilize the calculation process [14]. Other approaches to the regularization of the problem include: regularization through optimization of a discrete *f(r)* in a Monte Carlo search for the solution [15]; by model-based approaches approximating *f(r)* by the sum of a few Gaussian curves with non-linear least-squares methods [16]; and by Monte-Carlo [17] or non-linear least-squares methods with multiple starts [18]. The most commonly used program for data analysis is the DeerAnalysis software [19], which contains a standard Tikhonov algorithm and a few model-based algorithms with various peak functions. A Bayesian approach was recently proposed that explicitly uses the basic principles of Tikhonov regularization and information about the noise structure and noise level to obtain *f(r)* itself, and the magnitude of the error in *f(r)* [20]. Significant help is also provided by preliminary filtering of the signal; for example, with the help of wavelet transforms [21]. Combining wavelet filtering with singular value decomposition in PELDOR data inversion is suggested in [22].

View Article Online
DOI: 10.1039/C7CP04059H

We should understand that each approach possesses its own advantages and disadvantages for different types of distributions, because each set of regularizing assumptions can distort real distributions in different manners.

Exact analytical solution

We present here an ideologically new approach, based on an exact analytical solution of Eq.(1). First, let us rewrite Eq.(1) in the following form for convenience by replacing the variables r and θ with equivalent variables $w = \gamma^2 \hbar / r^3$ and $x = cos\theta$, using $p(w)dw = f(r)dr$. The functions *p(w)* and *f(r)* are related by the Jacobians (see Appendix).

$$V(T) = \int_0^\infty \int_0^1 p(w)\cos(wT(1-3x^2))dxdw \tag{2}$$

In some special cases one should consider correlations between the variables r and θ (equivalent variables w and x), a condition called orientation selection [5, 23] which introduces a geometrical form-factor into the kernel [24]. In the absence of such correlations, the variable x can be eliminated,

$$V(T) = \int_0^\infty \int_0^1 p(w)\cos(wT(1-3x^2))dxdw = \int_0^\infty p(w)\varphi(w,T)dw$$

$$\varphi(w,T) = \int_0^1 \cos(wT(1-3x^2))dx = \sqrt{\frac{\pi}{6}}\frac{\cos(wT)\,C\left(\sqrt{6wT/\pi}\right) + \sin(wT)\,S\left(\sqrt{6wT/\pi}\right)}{\sqrt{wT}} \tag{3}$$

where S(x) and C(x) are the Fresnel functions. And finally we have

$$V(T) = \int_0^\infty p(w)\varphi(wT)dw \tag{4}$$

Now, the functional dependence of the kernel on the variables is clearly seen: $\varphi(w,T) = \varphi(wT)$. Conversion of Eq.(1) to this form allows us to solve the equation analytically through the integral Mellin transform [25]. This transform is defined as

$$Y(s) = \int_0^\infty y(x)x^{s-1}dx \tag{5}$$

where the variable s is complex and dimensionless. The Mellin transform allows separation of the variables w and T. Indeed, application of this transform to Eq. (4) gives us

$$\int_0^\infty V(T)T^{s-1}dT = \int_0^\infty \int_0^\infty p(w)\varphi(wT)\,T^{s-1}dTdw \tag{6}$$

To separate the variables, let us make a replacement $y = wT$ then $T^{s-1} = (y/w)^{s-1}$ and $dT = (1/w)dy$:

$$\int_0^\infty V(T)T^{s-1}dT = \int_0^\infty \int_0^\infty p(w)\varphi(wT)\,(y/w)^{s-1}\big((1/w)dy\big)dw \tag{7}$$

$$\int_0^\infty V(T)T^{s-1}dT = \int_0^\infty p(w)w^{-s}dw \int_0^\infty \varphi(y)y^{s-1}dy \tag{8}$$

View Article Online
DOI: 10.1039/C7CP04059H

Thus, we get $\tilde{V}(s) = P(1-s)\Phi(s)$, where $\tilde{V}(s)$ is Mellin image of an experimental signal $V(T)$ and $\Phi(s)$ is the Mellin image of the kernel function $\varphi(wT)$.

Consequently,

$$P(s) = \frac{\tilde{V}(1-s)}{\Phi(1-s)} \quad (9)$$

Applying the inverse Mellin transform to (9), we finally obtain a solution

$$p(w) = \frac{1}{2\pi i}\int_{c-i\infty}^{c+i\infty} P(s)w^{-s}ds \quad (10)$$

Practical use of the exact solution faces difficulties due to instability of the initial equation. The Mellin spectrum of the kernel or, equivalently, the Mellin spectrum of $V(T)$ with $f(r) = \delta(r-r_0)$ can be calculated analytically, for example, by mathematical software Wolfram Mathematica 7.0 in terms of generalized hypergeometric functions [26] (see Appendix). But if $f(r) \neq \delta(r-r_0)$ then the Mellin spectrum of $V(T)$ must be calculated numerically, with some regularizing assumptions.

Numerical algorithm

The first step is to find the Mellin transform, $\tilde{V}(s)$, of the experimental signal.

$$\tilde{V}(s) = \int_0^\infty V(T)T^{s-1}dT.$$

For integration in $L^2(0,\infty)$ space it is suitable to use

$$s = \frac{1}{2} + i\tau. \quad (11)$$

Our choice of the constant c = 1/2 is for convenience in the calculations. The variable τ, like s, is still dimensionless. There are restrictions on c according to the criteria described in [27]. The restrictions for a kernel transform are stronger due to the obvious boundedness of the experimental $V(T)$, but to use Eq. 9 we must use the same c for the signal and the kernel transforms. It can be shown that the restrictions for the kernel transform, and therefore the general signal transform, are $0<c<3/2$, see Appendix. So, at c = 1/2 we get:

$$T^{s-1} = T^{-1/2}T^{i\tau} = \frac{1}{\sqrt{T}}\exp(i\tau\ln T) = \frac{1}{\sqrt{T}}(\cos(\tau\ln T) + i\sin(\tau\ln T)) \text{ and}$$

$$\tilde{V}(\tau) = \int_0^\infty V(T)\frac{1}{\sqrt{T}}\cos(\tau\ln T)dT + i\int_0^\infty V(T)\frac{1}{\sqrt{T}}\sin(\tau\ln T)dT \quad (12)$$

It can be seen that the functions $cos(\tau lnT)$ and $sin(\tau lnT)$ at small time T become very unpleasant, rapidly-oscillating functions, with the oscillation frequency increasing as $(\tau\ lnT)/T \approx \tau/T$ and with amplitude increasing as $\sim 1/\sqrt{T}$. Therefore, numerical integration near T=0 becomes quite difficult.

View Article Online
DOI: 10.1039/C7CP04059H

At the same time, it is very simple to demonstrate that our experimental function $V(T) \approx 1 + const * T^2$ as T approaches zero, and so it is changing relatively slowly. Therefore, it is suitable to split the integrals in eq. (12) into two parts:

$$\int_0^\infty V(T)\frac{1}{\sqrt{T}}exp(i\tau \ln T)dT \approx V(0)\int_0^\delta \frac{1}{\sqrt{T}}\exp(i\tau \ln T)dT + \int_\delta^\infty V(T)\frac{1}{\sqrt{T}}exp(i\tau \ln T)dT$$

The first part can be calculated analytically:

$$\int_0^\delta \frac{1}{\sqrt{T}}\exp(i\tau \ln T)dT = \int_0^\delta T^{-1/2+i\tau}dT = \frac{\delta^{\frac{1}{2}+i\tau}}{\frac{1}{2}+i\tau} \qquad (13)$$

while the second part becomes available for numerical integration. It should be noted that the divergence problem for eq. (12) from a rapidly oscillating $\exp(i\tau \ln T)$ occurs not only at low T, but also at large τ. Fortunately, $\tilde{V}(\tau)$ decays to zero before $\exp(i\tau \ln T)$ starts to rapidly oscillate and therefore we can choose a value of τ_{max} that allows us to avoid this problem (see Fig. 1a).

According to the accepted terminology [28], regularization of ill-posed problems consists of the use of additional *a priori* information. In this example, the explicit use of knowledge about $V(T \to 0)$ and we will see that this information really plays a regularizing role.

Let us demonstrate the application of our approach by a particular example with a model distance distribution, $f_0(r)$, consisting of two overlapping peaks - narrow and wide. We choose this type of distribution because of the well-known difficulties in applying the Tikhonov approach to such cases. A simulated PELDOR decay curve $V_0(T)$ was calculated from this model function $f_0(r)$ according to eq. (1) with r in nanometers:

$$f_0(r) = \frac{1}{2}\left(\frac{1}{0.1\sqrt{2\pi}}\exp\left(-\frac{(r-2)^2}{2\times 0.1^2}\right) + \frac{1}{0.4\sqrt{2\pi}}\exp\left(-\frac{(r-2.5)^2}{2\times 0.4^2}\right)\right) \qquad (14)$$

The integration range and the integration step (T_{max} and dT) were chosen so that the final results are fully converged. All numerical integrations were done using the Simpson rule [29].

We obtained the Mellin spectrum of the function $\tilde{V}(s)$, the Mellin spectrum of the kernel $\Phi(s)$ and, in accordance with eq. (9), the Mellin spectrum $P(s)$ of the desired distribution function. Recall that $s = \frac{1}{2} + i\tau$, so all the above quantities have complex values with real and imaginary parts.

The inverse Mellin transform can be done according to (10) also with $s = \frac{1}{2} + i\tau$.

$$p(w) = \frac{1}{2\pi i}\int_{1/2-i\infty}^{1/2+i\infty} P(s)w^{-s}ds = \frac{1}{2\pi}\int_{-\infty}^{+\infty} P(\tau)\, w^{-1/2-i\tau}d\tau = \frac{1}{2\pi}w^{-1/2}\int_{-\infty}^{+\infty} P(\tau)\, w^{-i\tau}d\tau,$$

$$Re[p(w)] = \frac{1}{2\pi}w^{-1/2}\int_{-\infty}^{+\infty} Re[P(\tau)]\cos(\tau lnw)d\tau - \frac{1}{2\pi}w^{-1/2}\int_{-\infty}^{+\infty} Im[P(\tau)]\sin(\tau lnw)d\tau$$

View Article Online
DOI: 10.1039/C7CP04059H

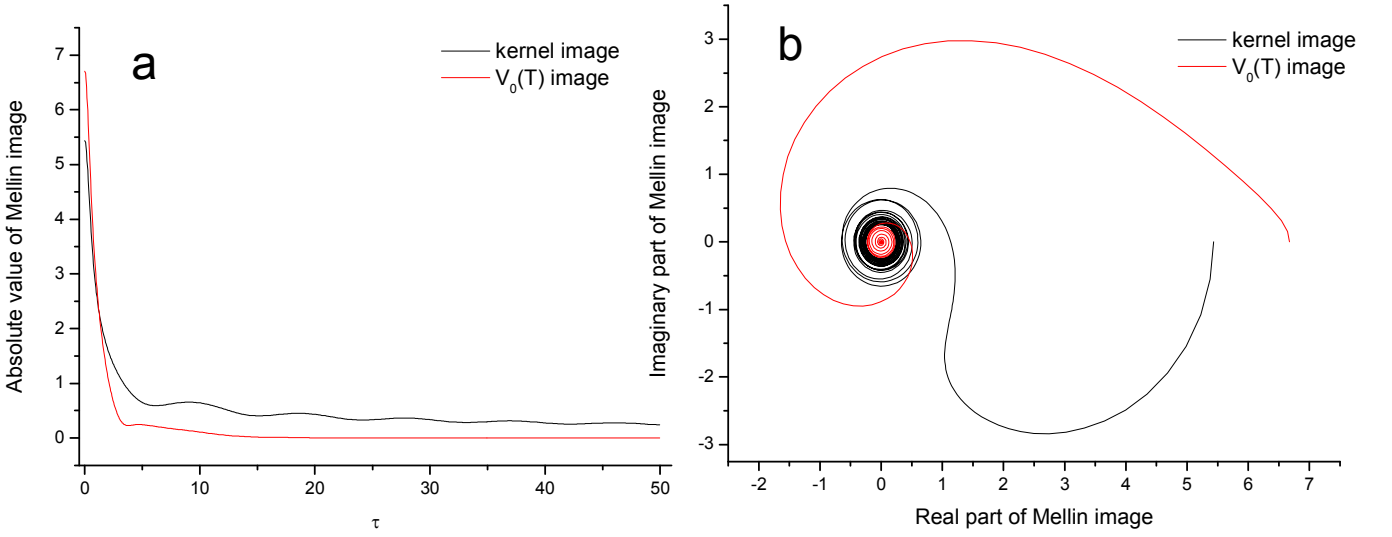

Fig.1 Mellin spectra of the kernel and $V_0(T)$ calculated from (14) according to eq. (1). a) Absolute value of $\Phi(\tau)$ and $\widetilde{V_0}(\tau)$ versus τ; b) $Im[\Phi(\tau)]$ versus $Re[\Phi(\tau)]$ and $Im[\widetilde{V_0}(\tau)]$ versus $Re[\widetilde{V_0}(\tau)]$. Note that the Mellin spectrum of the kernel is calculated analytically (see Appendix). Numerical integration would not be very good because of 'the window effect' - the kernel decreases very slowly and we can't choose a suitable T_{max} for integration.

It seems that here we face similar problems, but in fact the reverse integral transform is the opposite of the direct transform in many ways. Now, the integrand has a constant frequency $\ln w$ and therefore even at small w one can always find a reasonable $d\tau$, so that numerical integration does not cause any problems. It is possible to ignore very large w, where $\ln w$ becomes large, because they have no physical meaning.

Fig.2 demonstrates the recovery of $f(r)$ from our $V_0(T)$ for different levels of Gaussian noise. The noise was added to $V_0(T)$ and then $f(r)$ recovered using the proposed procedure. The results are shown in Fig. 2b and compared to the original $f_0(r)$. Table 1 shows parameters used in all numerical integrations.

Note that the Mellin spectrum of a function must be calculated with the same variable as the argument of studied function. That is, if the time in $V(T)$ is given in nanoseconds, then T in the integral (6) should also be taken in nanoseconds. In addition, if we want to obtain $f(r)$ in nanometers, the corresponding dimension must have the variable wT.

Table 1. Parameters used in numerical integrations. The numbers of points (Nr, N_T, N_τ and N_w for respective variables) and discretization steps for each integration are listed. They are sufficient for convergence to the final results. The optimized value of δ was δ=0.2 (see below)

N_r/dr for $f(r)$	N_T/dT for $V(T)$	N_T/dT for direct Mellin	$N_\tau/d\tau$ for direct Mellin	$N_\tau/d\tau$ for reverse Mellin	N_w/dw
909/0.05	35000/0.03	340000/0.003	1000/0.05	5000/0.01	1950/0.01

View Article Online
DOI: 10.1039/C7CP04059H

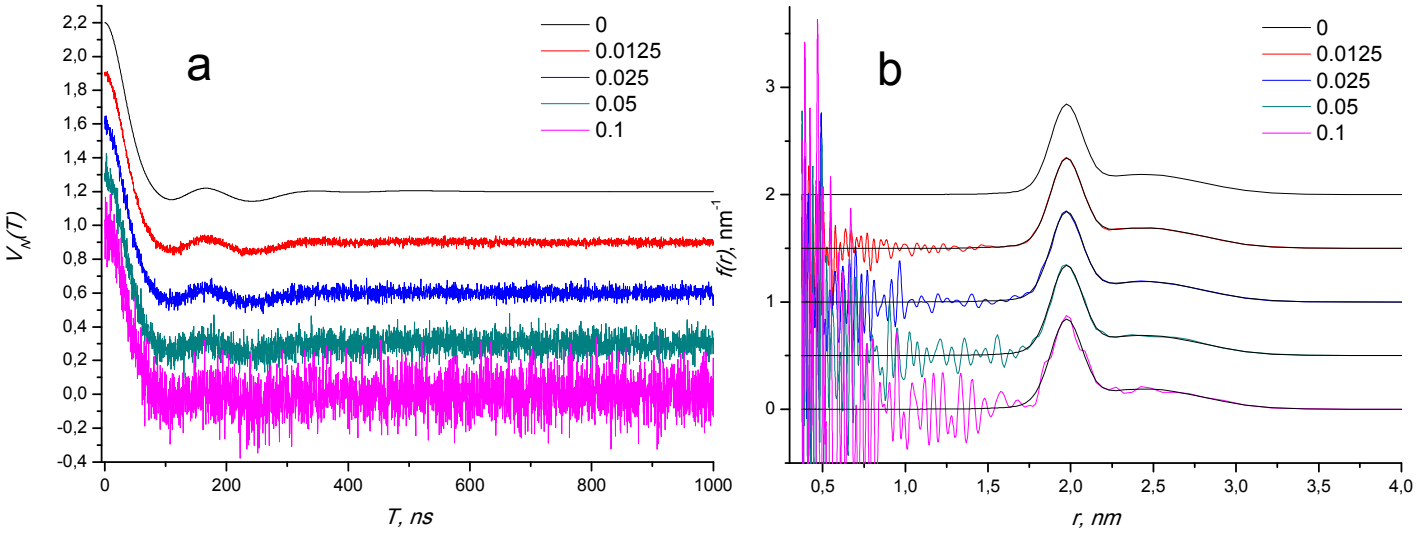

Fig.2 Quality of distance distribution recovery by the present algorithm: dependence of restored curve on noise level in input data. a – normalized PELDOR curves *V(T)* with different levels of noise calculated from $f_0(r)$ (value of standard deviation of Gaussian noise σ = 0, 0.0125, 0.025, 0.05 and 0.1); b –distance distribution, obtained from this *V(T)*.

Results and Discussion

It is seen (Fig.2b) that the function $f_0(r)$ is almost exactly reproduced in the absence of noise. There is only a minor deviation at extremely small distances, which is not visible in the figure. Increases of noise level in *V(T)* leads to an obvious decrease in accuracy of recovering *f(r)*. This effect is widely seen in all methods of solving such inverse problems, but there are two substantial differences in comparison, for example, with the Tikhonov approach.

The main difference is the very obvious grouping of noise at small distances, as seen in Fig.2b. In contrast, errors in the recovery of *f(r)* do not depend on the distance itself for the Tikhonov or any current approach. The proposed algorithm interprets any noise in *V(T)* as a correctly measured PELDOR signal and consistently gives many false peaks at short distances. This noise grouping effect is very attractive because the distance range accessible to the PELDOR technique is bounded from below. That is, PELDOR cannot measure very short distances anyway due to the microwave pulse bandwidth limitations and due to physical limitations of Eq. (1) at short distances, for example, by the exchange interaction.

View Article Online
DOI: 10.1039/C7CP04059H

The second important feature of our algorithm is that the additivity between signal and noise in the time domain carries over to the distance domain. Indeed, all the procedures: direct Mellin transform, use of Eq. (9) and reverse Mellin transform, are linear additive procedures. Therefore, from $V(T)=V_0(T)+noise$ we will obtain $f(r)=f_0(r)+noise'$. Our algorithm, as opposed to Tikhonov regularization, preserves the shape of $f_0(r)$ despite the level of noise, and recovers it quite acceptably even with a high noise level, particularly in the region of large r. It can be easily demonstrated that these false peaks accurately reproduce the noise in $V(T)$ when the noisy $f(r)$ is used in Eq. (1). This additivity is an important property, which avoids specific problems in obtaining distance complicated distributions – the proposed algorithm does not introduce a systematic error in the recovered distribution function. It does not broaden narrow signals, does not merge the two peaks of a bimodal distribution into one wide peak, etc. In short, unlike all current approaches, our proposed method provides an unbiased distance distribution.

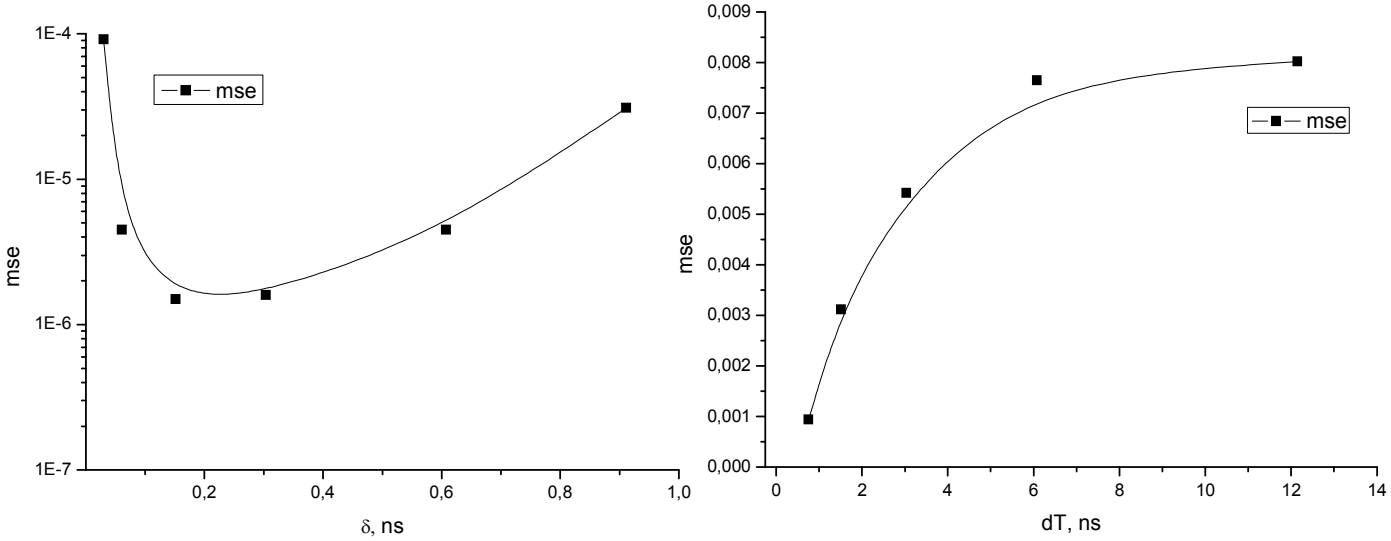

Fig. 3 Dependence of mean square error between input and restored $f(r)$ over the distance range between 1.5 and 5.85 nm: a) on the value of the regularizing parameter δ for noise-free data, b) on the discretization length dT in calculated $V(T)$ (for data with a noise level of $\sigma = 0.01$).

One can see that these advantages of our approach come from internal properties of the problem and result from the use of an analytical solution with minimum *a priori* assumptions. Now we must comment about regularization in the algorithm. The Mellin spectrum (see Fig.1) can be described as a representation in the space of continuous powers. Our method of calculating such a spectrum of $V(T)$ replaces the contribution at very small times by a constant value and does reject the contributions from very high powers. It conceptually resembles zero filling and subsequent rejection of high frequencies in the Fourier transform $V(T)$ of a Pake doublet and plays a regularization role in the solution of the inverse problem.

View Article Online
DOI: 10.1039/C7CP04059H

Fig. 3a shows a plot of the logarithm of mean square deviation between initial and restored *f(r)* versus parameter δ. It can be seen that there is a wide range for δ optimal values. The character of this dependence really allows us to think of δ as a regularizing parameter in the present approach [28]. Indeed, the δ-curve from the Fig.3a has the same sense as *L*-curve in the standard Tikhonov algorithm [12, 19]. In practice, instead of the δ-curve, we can recommend a simple estimate from $V(\delta) \approx 0.95$.

Comparison with other methods and evaluation of errors

Consider the experimental example of the bimodal distribution obtained in article [17] for biradical II-10 with non-rigid labels of the TEMPO type attached to the base of the trolox, a synthetic analogue of vitamin E. The experiment was done in X band by a three-pulse sequence of 16ns-32ns observer pulses and a 28 ns pump pulse whose position was incremented in steps of 4 ns, for more detail see [17]. Figure 4a shows the result of processing the experiment II-10 by three methods: the standard Tikhonov regularization (blue curve); as approximated by four Gaussians as suggested in [17] (the black curve); and the solution obtained by the proposed algorithm (red curve). Parameters used for the Mellin-based calculation are identical to Table 1. Figure 4b shows the *L*-curve produced by the DeerAnalysis software, which demonstrates the limitations of the Tikhonov algorithm [19] for this data. It is seen that for this experiment the dependence of the mean square deviation on smoothness does not have an inflection, and therefore the function *f(r)* can be chosen only with some additional information, for example, from the results of model-based fitting. Other approaches have been made using Marquardt-Levenberg optimization in DeerAnalysis [19] with a sum of two Gaussians or using a Monte-Carlo search with optimization of the number of Gaussians [17]. On the other hand, any model approach is obviously limited by the choice of model - for example, with a high noise level it is difficult to understand how many Gaussian functions should be chosen for an adequate description of the experiment. We think that Fig.4 demonstrates the need for an integrated approach to solving the inverse problem of PELDOR - Tikhonov and model-based approaches allow us to look at the situation using different filters, and Mellin-based approach allows us to see the limit of the permissible accuracy in assessing this situation. The advantage of the approach proposed is that it explicitly shows which information one can reliably extract from the experiment. In this example, we can reliably distinguish two peaks - about 1.5 and about 1.8 nm, and we can determine the width and position of the second peak almost exactly, but we can only talk about the width and position of the first peak with some degree of uncertainty.

View Article Online
DOI: 10.1039/C7CP04059H

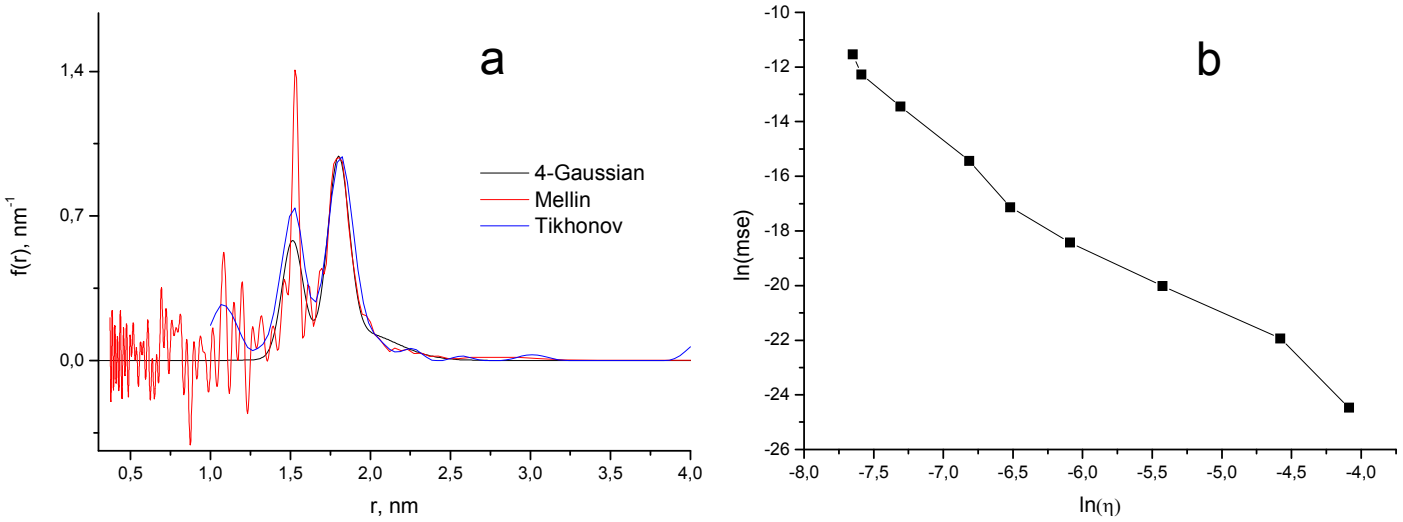

Fig.4 a - Comparison of distance distribution functions obtained for II-10 [17] in three approaches: 4-Gaussian Monte-Carlo search, suggested Mellin transform based approach, and Tikhonov regularization; b – corresponding *L*-curve (parametrical dependence of mean square error of approximation on its smoothness)

It is seen that in the short distance region our algorithm produces significant error, but the error explicitly reflects the intrinsic properties of the problem and the amount and quality of available experimental information. Indeed, the error in the recovered *f(r)* depends on general parameters – level of the noise and time step of sampling. Fig.2 demonstrates effect of noise level. The use of a large time step is obviously equivalent to loosing information about the system and leads to increased instability in the reverse problem [30]. Figure 3b and Figure 5 demonstrate the impact of the time step in the proposed algorithm. If we use the same *V(T)*, but different values of *dT*, then the well-defined area of *f(r)* will shorten and shift to larger *r*. It is clear because noise in *V(T)* is understood as rapid oscillations from many narrow peaks at small *r*. Therefore increasing the value of *dT* leads to a corresponding shift of the false peak region to larger *r*. Note that changes in discretization length may change only the location of the false peaks and nothing more – the shape of the real $f_0(r)$ remains unchanged. Thus, the area of the false peaks is a partially-blind spot where the underlying, accurate $f_0(r)$ could be recovered using additional *a priori* information or assumptions. We note that the magnitude of this error depends only on the above mentioned *V(T)* parameters and does not depend on the distribution function $f_0(r)$ itself.

View Article Online
DOI: 10.1039/C7CP04059H

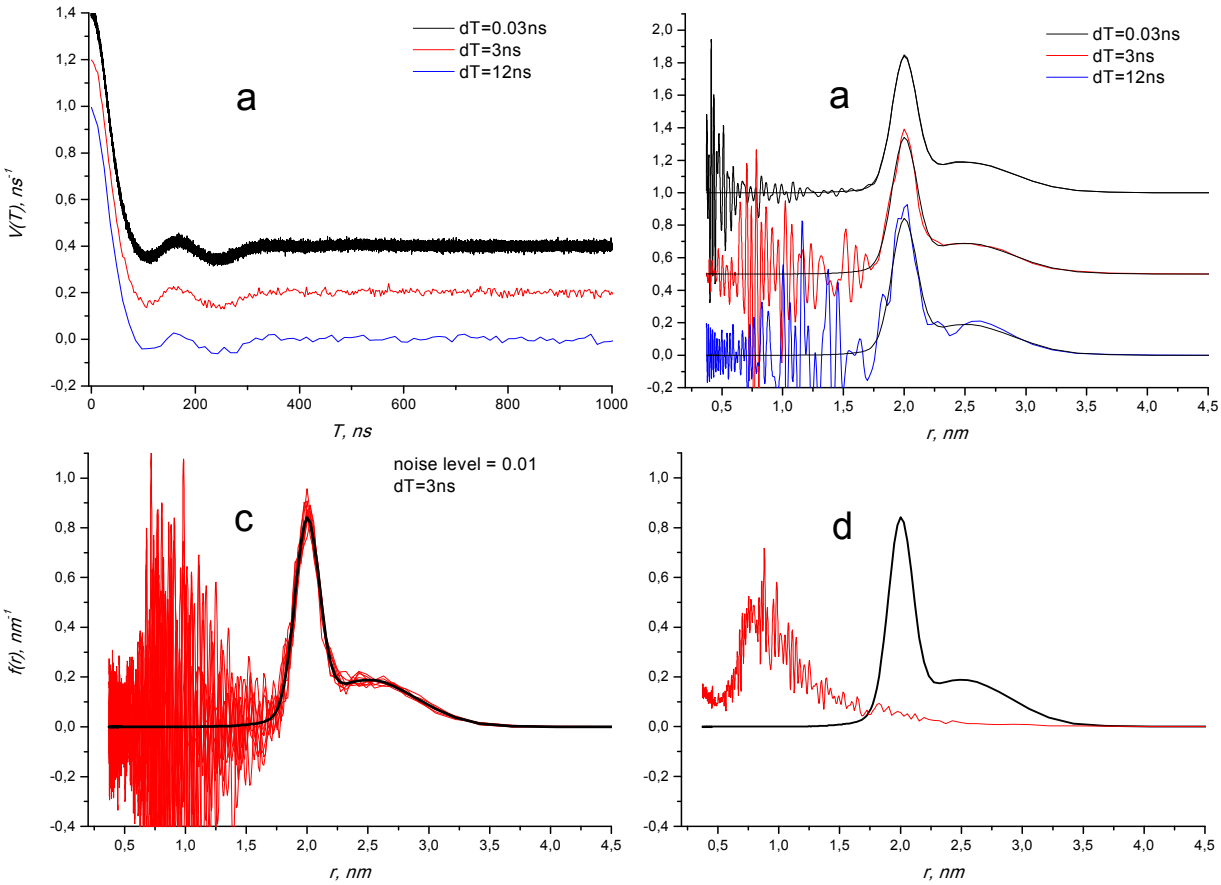

Fig. 5 Quality of the recovered distance distribution for the present algorithm: dependence of the recovered curve on discretization length *dT* in input data (obtained at noise level σ = 0.01). a – *V(T)* with different *dT* = 0.03, 3 and 12ns; b – corresponding recovered *f(r)*; c – 9 different *f(r)*, obtained from same *V(T)* with *dT*=3ns with different realization of Gaussian noise; d – root-mean-square error calculated from Fig. 5c.

If the noise in *V(T)* has a mean value of zero, then the noise in the recovered *f(r)* also has a mean value of zero (see Fig.5c). This fact can help estimate the size of the blind spot in noisy *f(r)*, but we can recommend estimating the blind spot in the experimental data not only by eye, but by solving the inverse problem for pure noise, without a signal. To do this, one needs to have a noise recorded under the same conditions as the signal, as is done, for example, in a procedure for correcting artifacts [31].

Finally, we should remark about other problems which can be solved by this approach. Very similar inverse problems exist in searching for distance distributions between spins from out-of-

View Article Online
DOI: 10.1039/C7CP04059H

phase ESE experiments. In the point dipolar approximation there is an integral equation (in the authors' designation) [32]:

$$M_X(\tau) = \int\int G(r)\sin(\frac{\gamma^2\hbar}{r^3}(1-3\cos^2\theta)\tau)\sin\theta d\theta dr$$

where $M_x(\tau)$ is the experimental signal and $G(r)$ is the unknown distance distribution. The Mellin spectrum of this sine function-kernel can be done analytically and expressed in terms of generalized hypergeometric functions as was done for the cosine-kernel from Eq. (1).

Sometimes FRET spectroscopy also needs solutions of the Fredholm integral equation of the first kind for the distance distribution functions $p(r)$ between the donor and acceptor of energy. In the point dipolar approximation and in the absence of orientation selectivity there is an integral equation (in the authors' designation) [33]:

$$F_{DA}(t) = \int_0^\infty p(r)\exp\left(-\frac{t}{\tau_0}\left[1+\left(\frac{R_0}{r}\right)^6\right]\right)dr$$

It seems to be acceptable to use Mellin transform to solve this equation because it is simple to obtain the Mellin image of the kernel,

$\int_0^\infty \exp(-\frac{t}{\tau_0}[1+\left(\frac{R_0}{r}\right)^6]) * t^{s-1}dt = \Gamma[s]\left(\frac{1}{\tau_0}+\frac{R_0^6}{\tau_0}\right)^{-s}$ if $\mathrm{Re}[s] > 0$, $\Gamma[s]$ is a gamma-function. The Mellin transform was successfully used to solve similar equations with an exponential kernel [30].We speak about this problem here because of the appearance of new research containing PELDOR and FRET comparison in the field of distance measurements [34-36].

Conclusion

An exact analytical solution of the PELDOR inverse problem for doubly spin-labelled molecules was obtained in the absence of exchange interactions and orientation selection. Using a non-standard regularization technique, we developed a numerical algorithm to find the distance distribution function without *a priori* assumptions about the form of this distribution. The proposed algorithm does not distort the shape of the distribution function, but contains false peaks in the region of small distances. The position and intensity of these false peaks depend on the noise level and the length of the sampling step of the time-domain dipolar evolution signal. The proposed approach can be useful for investigation of a wide range of doubly spin-labelled systems, from proteins and antimicrobial peptides [37] through RNA duplexes [11] to DNA cocaine aptamers [38].

Acknowledgements

We gratefully thank Michael K. Bowman, Sergei A. Dzuba, Sergei I. Trashkeev and Victoria N. Syryamina for fruitful comments and useful considerations with special thanks to Alexander E.

View Article Online
DOI: 10.1039/C7CP04059H

Mamontov for considering fine features of the Mellin transform. This work was partly supported by the Russian Science Foundation, A.G. Matveeva thanks project # 15-15-00021.

Appendix

The functions *p(w)* and *f(r)* are related by the Jacobians:

$$p(w) = f\big(r(w)\big)\frac{dr(w)}{dw} = f\big((\gamma^2\hbar/w)^{-1/3}\big) * \left(-\frac{1}{3} * \frac{(\gamma^2\hbar)^{1/3}}{w^{4/3}}\right)$$

$$f(r) = p\big(w(r)\big)\frac{dw(r)}{dr} = p(\gamma^2\hbar/r^3) * \left(-3 * \frac{\gamma^2\hbar}{r^4}\right)$$

An analytical expression for the Mellin transform of the kernel is

$$\Phi(s) = \int_0^\infty \varphi(wt)\times(wt)^{s-1}d(wt) = \sqrt{\frac{\pi}{6}}\int_0^\infty \frac{\cos(y)C[\sqrt{6y/\pi}]+\sin(y)S[\sqrt{6y/\pi}]}{\sqrt{y}}\times y^{s-1}dy =$$

$$= \frac{3^{-s}\cos[\frac{\pi s}{2}]\Gamma[s]\ {}_3F_3[\{-\frac{1}{4}+\frac{s}{2},\frac{1}{2}+\frac{s}{2},\frac{s}{2}\},\{\frac{1}{2},\frac{3}{4}+\frac{s}{2}\},\frac{1}{9}]}{1-2s} +$$

$$+\frac{3^{1-s}\cos[\frac{\pi s}{2}])\Gamma[1-s]\ {}_3F_3[\{\frac{1}{4}+\frac{s}{2},\frac{1}{2}+\frac{s}{2},1+\frac{s}{2}\},\{\frac{3}{2},\frac{5}{4}+\frac{s}{2}\},\frac{1}{9}]}{1+2s} + \frac{\sqrt{3\pi}}{6}\Gamma[s-\frac{1}{2}]\sin[\frac{\pi s}{2}]$$

where *C(z)* and *S(z)* are Fresnel integrals, $\Gamma[s]$ is the gamma-function and ${}_3F_3[a,b,z]$ is the generalized hypergeometric function. Analytical solution exists if $0 < \mathrm{Re}[s] < 3/2$. These limitations can be easy understood by considering the short-time and long-time approximation of the kernel [39]: $\varphi(w, T \to 0) \approx 1 + O(T^2)$ and $\varphi(w, T \to \infty) \sim \frac{1}{\sqrt{T}}\cos(wT + \frac{\pi}{4})$.

View Article Online
DOI: 10.1039/C7CP04059H

References

1. A.D. Milov, K.M.Salikhov, M.D. Shirov, *Fiz. Tverd. Tela*, 1981, **23**, 975-982.
2. M. Pannier, S. Veit, A. Godt, G. Jeschke, H.W. Spiess, *J. Magn. Reson.*, 2011, **213**, 316–325.
3. P.P. Borbat, E.R. Georgieva, J.H. Freed, *J. Phys. Chem. Lett.*, 2013, **4**, 170–175.
4. B.Joseph, V.M. Korkhov, M. Yulikov, G. Jeschke, E. Bordignon, *J. Biol. Chem.,* 2014, **289**, 3176-3185.
5. A. Marko, V. Denysenkov, D. Margraf, P. Cekan, O. Schiemann, S.Th. Sigurdsson, T.F. Prisner, *J. Amer. Chem. Soc.*, 2011, **133**, 13375–13379.
6. S. Böhme, H.-J. Steinhoff, J.P. Klare, *Spectroscopy*, 2010, **24**, 283–288.
7. I.D. Sahu, R.M. McCarrick, K.R. Troxel, R. Zhang, H.J. Smith, M.M. Dunagan, M. S. Swartz, P.V. Rajan, B.M. Kroncke, C.R. Sanders, G.A. Lorigan, *Biochem.*, 2013, **52**, 6627−6632.
8. H. Yagi, D. Banerjee, B. Graham, T. Huber, D. Goldfarb, G. Otting, *J. Am. Chem. Soc.*, 2011, **133**, 10418–10421.
9. Yu.D. Tsvetkov, A.D. Milov, A.G. Maryasov, *Russ. Chem. Rev.*, 2008, **77**, 487–520.
10. N.A. Kuznetsov, A.D. Milov, N.P. Isaev, Yu.N. Vorobjev, V.V. Koval, S.A. Dzuba, O.S. Fedorova and Yu.D. Tsvetkov, *Mol. BioSyst*., 2011, **7**, 2670–2680.
11. M.K. Bowman, A.G. Maryasov, N. Kim, V.J. DeRose, *Appl. Magn. Reson*., 2004, 26, 23–39.
12. Y.-W. Chiang, P.P. Borbat, J.H. Freed, *J. Magn. Reson.*, 2005, **172**, 279–295.
13. J.A. Jones, P.J. Hore, *J. Magn. Reson.*, 1991, **92**, 363-376.
14. Y.-W. Chiang, P.P. Borbat, J.H. Freed, *J. Magn. Reson.*, 2005, **177**, 184–196.
15. S.A. Dzuba, *J. Magn. Reson.*, 2016, **269**, 113–119.
16. S. Brandon, A.H. Beth, E.J. Hustedt, *J. Magn. Reson.*, 2012, **218**, 93–104.
17. A.G. Matveeva, Y.V. Yushkova, S.V. Morozov, I.A. Grygor'ev, S.A. Dzuba, *Z. Phys. Chem.*, 2017, **231**, 671–688.
18. K.I. Sen, T.M. Logan, P.G. Fajer, *Biochemistry,* 2007, **46***,* 11639-11649.
19. G. Jeschke, V. Chechik, P. Ionita, A. Godt, H. Zimmermann, J. Banham, C. R. Timmel, D. Hilger, H. Jung, *Applied Magn. Reson.* 2006, **30**, 473-498.
20. T.H. Edwards, S. Stoll, *J. Magn. Reson.*, 2016, **270**, 87–97.
21. M. Srivastava, E.R. Georgieva, J.H. Freed, *J. Phys. Chem. A*, 2017, **121**, 2452–2465.
22. M. Srivastava, J.H. Freed, *J. Phys. Chem. Letters*, 2017, **8**, 5648–5655.
23. R.G. Larsen, D.J. Singel, *J. Chem. Phys.*, 1993, **98**, 5134-5146.
24. A.G. Maryasov, Yu.D. Tsvetkov, J. Raap, *Applied Magn. Reson.*, 1998, **14**, 101-113.
25. A.D. Polyanin, A.V. Manzhirov. Handbook of integral equations. - 2nd ed. - Boca Raton: Chapman & Hall/CRC, 2008.
26. G. Fikioris, IEEE Trans. Antennas & Propagation, 2006, **54**, 3895-3907.
27. G. Alvarez, G. Cvetič, B.A. Kniehl, I. Kondrashuk, I. Parra-Ferrada, *arxiv:1611.08787*.
28. A.N. Tikhonov, A. Goncharsky A., V.V. Stepanov, A.G. Yagola, Numerical Methods for the Solution of Ill-posed Problems. Dordrecht: Kluwer Academic 1995.
29. C.W. Clenshaw, A.R. Curtis, *Numerische Mathematik*, 1960, **2**, 197-205.

View Article Online
DOI: 10.1039/C7CP04059H

30. L. Venkataramanan, T.M. Habashy, D.E. Freed, F.K. Gruber, *J. Magn. Reson.*, 2012, **216**, 43–52.
31. A.D. Milov, Yu.A. Grishin, S.A. Dzuba, Yu.D. Tsvetkov, *Applied Magn. Reson.*, 2011, **41**, 59-67.
32. S.A. Dzuba, P. Gast, A.J. Hoff, *Chem. Phys. Letters*, 1995, **236**, 595-602.
33. H. Höfig, M. Gabba, S. Poblete, D. Kempe, J. Fitter, *Molecules,* 2014, **19**, 19269-19291.
34. R.V. Agafonov, I.V. Negrashov, Y.V. Tkachev, S.E. Blakely, M.A. Titus, D.D. Thomas, and Y.E. Nesmelov, *PNAS,* 2009, **106**, 21625–21630.
35. D. Klose, J.P. Klare, D. Grohmann, C.W.M. Kay, F. Werner, H.-J. Steinhoff, *PLoS ONE,* 2012, **7**, 39492.
36. C. M. Grytz, S. Kazemi, A. Marko, P. Cekan, P. Güntert, S. Th. Sigurdsson, T. F. Prisner, *Phys. Chem. Chem. Phys.*, 2017, Advance Article, DOI: 10.1039/C7CP04997H
37. A.D. Milov, A.G. Maryasov, Yu.D. Tsvetkov, J. Raap, *Chem. Phys. Letters* 1999, **303**, 135-143.
38. C.M. Grytz, A. Marko, P.Cekan, S.Th. Sigurdsson, T.F. Prisner, *Phys. Chem. Chem. Phys.*, 2016, **18**, 2993-3002.
39. K. M. Salikhov, I. T. Khairuzhdinov, R. B. Zaripov, *Applied Magn. Reson.*, 2014, **45**, 573–619.

View Article Online
DOI: 10.1039/C7CP04059H

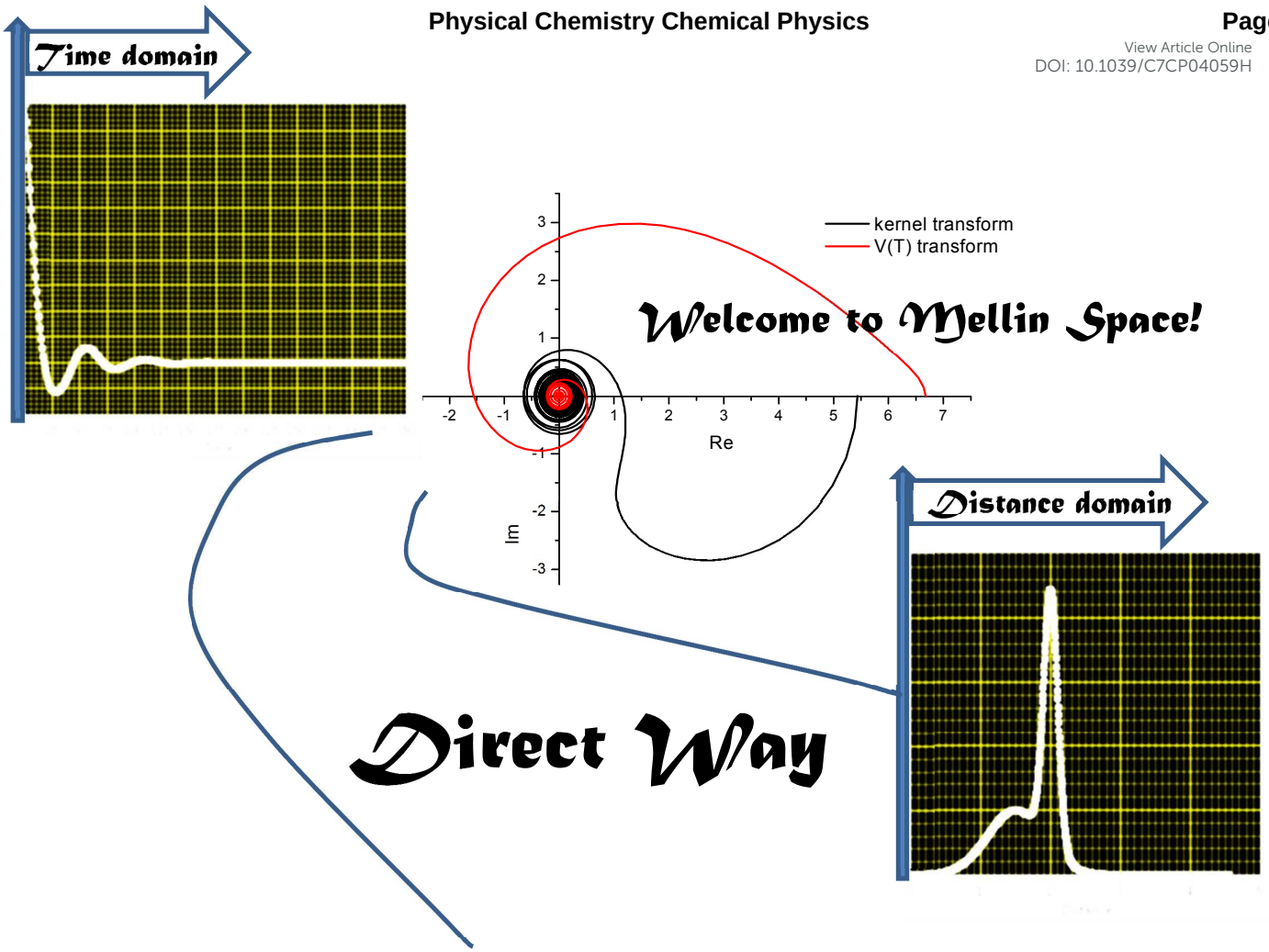

The model-free approach used does not introduce systematic distortions in the computed distance distribution function between two spins and appears to result in the noise grouping at the short distances range.